Editors' Suggestion

High-precision measurement of the Ferrell-Glover-Tinkham sum rule in a cuprate high-temperature superconductor

R. D. Dawson,[1,*] X. Shi,[1] K. S. Rabinovich,[1] D. Putzky,[1] Y.-L. Mathis,[2] G. Christiani,[1] G. Logvenov,[1] B. Keimer,[1] and A. V. Boris[1,†]

[1]*Max Planck Institute for Solid State Research, Heisenbergstraße 1, 70569 Stuttgart, Germany*

[2]*Institute for Beam Physics and Technology, Karlsruhe Institute of Technology, 76344 Eggenstein-Leopoldshafen, Germany*

(Received 22 March 2023; accepted 20 July 2023; published 5 September 2023)

The Ferrell-Glover-Tinkham (FGT) sum rule in superconductors defines the superfluid density, ρ_s, as the optical conductivity spectral weight (SW) that transfers into a δ function at $\omega = 0$ due to the opening of the energy gap below T_c. In high-T_c superconductors, strong electron-boson coupling, self-energy effects, and intertwining of energy scales can link ρ_s to various high-energy processes, making the question of whether or not the FGT sum rule is valid in cuprates, and at what energy scale, central to a full understanding of the pairing mechanism. Here, we report high-precision measurements of the FGT sum rule in near-optimally doped $DyBa_2Cu_3O_{7-\delta}$ thin films. We resolve the low-energy balance of SW by combining submillimeter-microwave interferometry, terahertz time-domain spectroscopy, and infrared ellipsometry to independently obtain the real and imaginary parts of the complex dielectric function between 0.8 meV and 1.1 eV (6–9000 cm^{-1}). By applying a Kramers-Kronig consistency analysis to the measured spectra we find that the FGT sum rule is obeyed, and the total intraband SW is conserved to within $\pm 0.2\%$ below an energy scale $\sim$0.6 eV. We attribute specific anomalies observed in the conductivity spectra below $\sim$0.6 eV to coupling of charge carriers to the spectrum of collective antiferromagnetic spin fluctuations. The procedure presented here, applied to near-optimally doped $DyBa_2Cu_3O_{7-\delta}$, lays out a protocol for how the FGT sum rule should be studied in other doping levels and compounds.

DOI: 10.1103/PhysRevB.108.104501

I. INTRODUCTION

On very general grounds, any microscopic theory that successfully describes superconductivity must allow for sum rules that link the energy gap function, $\Delta(\omega, \mathbf{k})$, to changes in the electrodynamic response across the transition temperature, T_c [1–3]. These sum rules encode information about the relationship between the superconducting order parameter, the magnetic penetration depth, and the electronic behavior in the normal state. By assessing their conditions of validity, as well as their frequency and temperature dependence, the sum rules provide insight into the nature of the superconductivity and the energy scale of the electron-electron pairing interaction [4].

The optical conductivity of a material in the superconducting state is defined by a δ-function component at $\omega = 0$, which describes the contribution from the superconducting charge carrier condensate, and a response at finite frequencies from charge carriers remaining in the normal, or uncondensed, state. Optical conductivity spectral weight (SW) shifts away from low frequencies (typically in the terahertz to far-infrared spectral range) as temperature is lowered below T_c and the energy gap $\Delta(\omega, \mathbf{k})$ opens. Following the development of BCS theory, Ferrell, Glover, and Tinkham (FGT) proposed a sum rule [5,6] that equates the SW lost from finite frequencies below T_c to the strength of the condensate δ function at the origin in terms of the superfluid density ρ_s,

$$\rho_s = \int_{0^+}^{\Omega_c} [\sigma_{1,n}(\omega) - \sigma_{1,s}(\omega)] d\omega = \frac{c^2}{8\lambda_L^2}, \tag{1}$$

where $\sigma_{1,n}(\omega)$ is the real part of the optical conductivity in the normal state, $\sigma_{1,s}(\omega)$ is the same in the superconducting state, and λ_L is the London penetration depth. Eliashberg theory, a many-body Green's function approach that provides a quantitative description of the electrodynamics of superconductors, gives the electron-boson self-energy and defines the upper integration bound Ω_c through the cutoff of the boson spectral function [7–10]. The validity of the FGT sum rule in a wide range of materials [2] and its connection to specific features in the optical conductivity related to the electron-phonon spectral density [11–13], $\alpha^2 F(\omega)$, provided strong quantitative support to the BCS theory and energy gap model of superconductivity.

Having been successful in accounting for the optical properties of conventional superconductors, this approach remains much more challenging in the cuprate high-temperature superconductors (HTSCs) due to the presence of various competing orders and strong correlations [14,15].

*rdaviddawson1@gmail.com

† A.Boris@fkf.mpg.de

In particular, the possible spin-fluctuation pairing mechanism suggests much higher energy scales for the electron-boson spectral function and Ω_c compared to phonon-mediated superconductivity [16]. Moreover, any superconductivity-induced optical response observed beyond Ω_c provides possible evidence for the violation of the FGT sum rule, which has been interpreted as an argument in support of unconventional (e.g., kinetic energy driven) pairing scenarios [17–26]. It is difficult to establish, however, that high-energy anomalies below T_c are related to the superfluid density rather than to superconductivity-induced changes in the scattering rate of unpaired quasiparticles [27,28] or multiband effects [29–31]. The validity of the FGT sum rule therefore cannot be established solely on the basis of spectra measured at or above the plasma edge [19,21,22,24,32–37]. Direct measurements of the complex electrodynamic response reaching to very low energies are needed to accurately determine the proper distribution of SW between the superconducting δ function and the quasiparticle response. Such experiments are challenging, however, because typical low-energy measurements are fragmentary and require extrapolation between experimentally accessible spectral ranges. The low-energy extrapolation of the dynamic response in the superconducting state of d-wave cuprate HTSCs is not straightforward due to the presence of competing orders and quantum criticality [15]. Moreover, at finite temperatures the narrow quasiparticle absorption peak remains, as evident from gigahertz surface impedance measurements down to 1.3 K [28]. This uncertainty becomes even more critical if only the amplitude and not the phase of the reflected or transmitted electromagnetic wave is measured and the Kramers-Kronig (KK) relations are used to derive the complex conjugate quantities.

To properly address the question of the validity of the FGT sum rule in the cuprates, fully phase-sensitive techniques spanning the complete intraband response from 1 eV down to less than 1 meV are required to remove the dependence of the analysis on the details of the low-energy extrapolation. Such techniques allow the real and imaginary parts of the complex dielectric function to be extracted independently while the causality implicit in the KK relations strongly bounds the accumulation of quasiparticle SW as $\omega \to 0$. By combining several phase-sensitive spectroscopic techniques in a unique way, we directly obtained broadband measurements of the complex dielectric function from the microwave to the near-infrared portion of the electromagnetic spectrum. These measurements have recently become available due to advances in terahertz generation and detection, which allow the terahertz spectral gap to be bridged by high-resolution time-domain spectroscopy. We find the FGT sum rule to be valid to within an unprecedented accuracy of 2%, leaving the total intraband SW unchanged in the superconducting state with an accuracy of 0.2% or 0.01 eV^2. This rules out unusual kinetic energy saving pairing mechanisms in optimally doped $RBa_2Cu_3O_{7-\delta}$ cuprates (RBCO, where R = rare earth), in agreement with Ref. [38]. We also find the cutoff of the FGT sum rule, $\Omega_c \sim 0.6$ eV, and observe specific features in the optical conductivity consistent with the known resonance energy and spectrum of spin excitations. The procedure and results presented here lay out a protocol for how the FGT sum rule should be accurately studied in other doping levels and compounds.

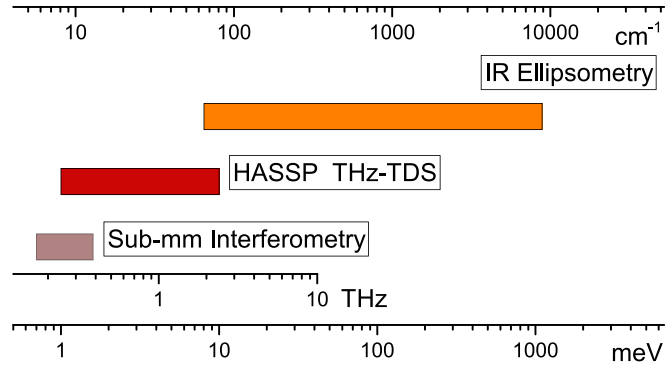

FIG. 1. A schematic of the spectral range used in this experiment. Broadband conductivity spectra between 0.8 meV and 1.1 eV were obtained by combining submillimeter-microwave interferometry, terahertz time-domain spectroscopy, and infrared spectroscopic ellipsometry. Spectra from each instrument were merged as described in Sec. II.

II. EXPERIMENTAL DETAILS

Thin films of c-axis-oriented, near-optimally doped $DyBa_2Cu_3O_{7-\delta}$ (DyBCO) 20 u.c. (23 nm, $T_c = 82$ K) and 60 u.c. (70 nm, $T_c = 90$ K) thick were grown on (100)-oriented $(LaAlO_3)_{0.3}(Sr_2AlTaO_6)_{0.7}$ (LSAT) substrates with dimensions 10×10 mm^2 by ozone-assisted atomic-layer-by-layer oxide molecular beam epitaxy. The high structural quality of the films was confirmed by x-ray diffraction, transmission electron microscopy, and transport measurements, as described elsewhere [39,40]. Broadband conductivity spectra between 0.8 meV and 1.1 eV (6–9000 cm^{-1}) were acquired by combining quasioptical submillimeter-microwave interferometry, terahertz time-domain spectroscopy (THz-TDS), and infrared spectroscopic ellipsometry as shown in Fig. 1. All optical measurements directly obtained both the real and imaginary parts of the complex dielectric function, $\tilde{\varepsilon}(\omega) = \varepsilon_1(\omega) + i\varepsilon_2(\omega) = 1 + 4\pi i[\sigma_1(\omega) + i\sigma_2(\omega)]/\omega$, in a temperature range from 7 to 300 K.

Infrared ellipsometry measurements were made in the range 8 meV to 1.1 eV (60–9000 cm^{-1}) with home-built ellipsometers at the MPI in Stuttgart and at the IR-1 beamline of the Karlsruhe Research Accelerator (KARA) at the Karlsruhe Institute of Technology, in conjunction with Bruker Vertex 80v and IFS 66v/s Fourier transform IR spectrometers, respectively. This method is very sensitive to the properties of thin films because of the oblique angle of incidence of the light [41]. The real and imaginary parts of $\tilde{\varepsilon}(\omega)$ in the ab plane were derived by numerical inversion of the ellipsometric angles Ψ and Δ, which were measured at an angle of incidence of 80° relative to the c axis, using a best-match single-film model calculation procedure as implemented in the Woollam WVASE data acquisition and analysis software [42].

High-resolution THz-TDS transmission spectra were measured in the spectral range 1–10 meV (8–80 cm^{-1}) with a LaserQuantum HASSP spectrometer utilizing the high-speed asynchronous optical sampling technique at a 1 GHz repetition rate. This system enabled effective scan rates of up to 5 kHz across a 1 ns measurement window with a corresponding spectral resolution of 1 GHz [43,44]. The complex dielectric function was calculated from the complex

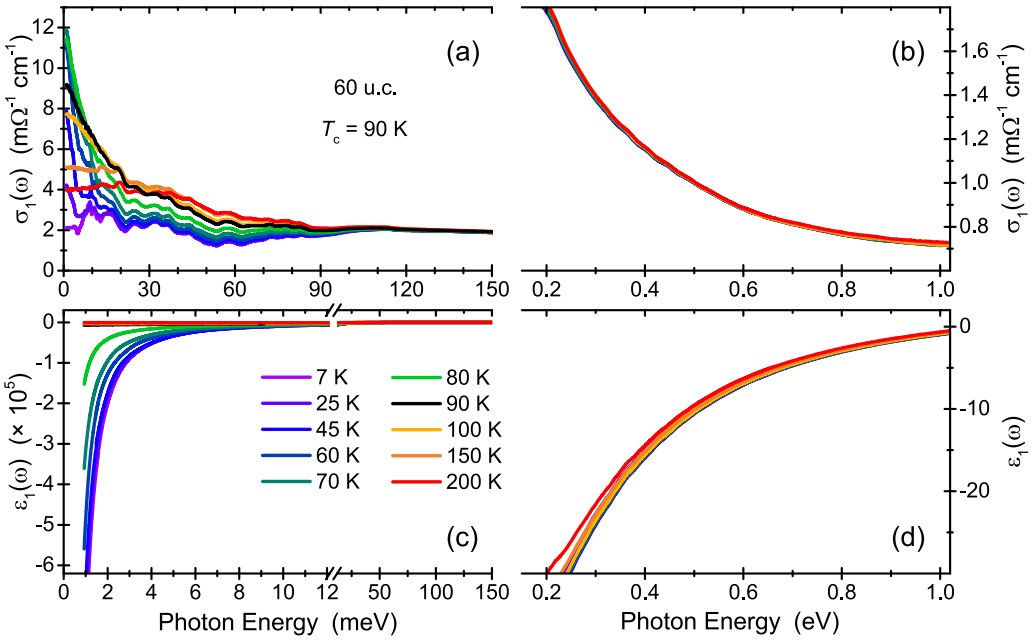

FIG. 2. The real part of the measured *ab*-plane optical conductivity (a), (b) and dielectric permittivity (c), (d) across the entire spectral range from 0.6 to 1.1 meV for a 60 u.c. thick DyBCO film, derived for a range of temperatures above and below $T_c = 90$ K. The spectra were measured using quasioptical submillimeter-microwave interferometry, THz-TDS, and infrared spectroscopic ellipsometry and merged together as described in Sec. II.

transmission, $\ln \tilde{T}(\omega) = \ln A(\omega) + i\phi(\omega)$, via inversion of the Fresnel coefficients for an electric field polarized parallel to the *ab* plane with a bare LSAT substrate used as a reference. A substrate thickness mismatch parameter ΔL was introduced as a free parameter to account for phase accumulation due to uncertainty in thickness between the sample and reference substrates. ΔL was adjusted until both $\varepsilon_1(\omega)$ and $\varepsilon_2(\omega)$ were simultaneously anchored to the infrared ellipsometry spectra. The value of ΔL was typically within ± 3 μm, confirmed by Nikon MH-15 digital micrometer measurements and consistent with the substrate miscut error.

Quasioptical submillimeter-microwave transmission measurements were performed by means of a Mach-Zehnder interferometer in the energy range 0.8–1.6 meV (6–13 cm^{-1}) with a backward wave oscillator as the radiation source [45,46]. Both $\varepsilon_1(\omega)$ and $\varepsilon_2(\omega)$ were extracted by simultaneously fitting the amplitude and phase of the interference pattern with the Fresnel transmission equations for a two-layer system. Finally, all spectroscopic data were merged in a self-consistent way by enforcing the requirement that $\varepsilon_1(\omega)$ and $\varepsilon_2(\omega)$ are smooth and continuous across the entire measured spectrum with a single set of temperature independent analysis parameters for each measurement. The resulting data were analyzed by considering the difference spectra $\Delta\varepsilon_1(\omega)$ and $\Delta\sigma_1(\omega)$, which give the changes in the spectra at a temperature T compared with T_c. The systematic error bar does not exceed the noise level of the difference spectra, $\sim 1\ \Omega^{-1}\ \text{cm}^{-1}$, as seen, for example, in $\Delta\sigma_1(\omega)$ above 0.5 eV.

III. SUPERCONDUCTIVITY-INDUCED SW TRANSFER

The real parts of the *ab*-plane optical conductivity, $\sigma_1(\omega)$, and dielectric permittivity, $\varepsilon_1(\omega)$, across the entire measured spectral range for the 60 u.c. thick DyBCO film are shown in Fig. 2. A large amount of optical SW is observed to shift from terahertz and far-infrared energies below T_c, marking the opening of the superconducting gap in $\sigma_1(\omega)$. This SW shift is accompanied by a dramatic downturn in $\varepsilon_1(\omega)$ that is proportional to $-1/\omega^2$, which is indicative of the accumulation of SW into a δ function in $\sigma_1(\omega)$ at the origin and the formation of the superconducting condensate. However, $\sigma_1(\omega)$ remains finite down to the lowest frequencies and temperatures $T \ll T_c$, which is not easily explained by a simple *d*-wave picture [3]. The measured residual conductivity of our films in the superconducting state is in very good quantitative agreement with prior results for $YBa_2Cu_3O_{6.9}$ single crystals, where the residual in-gap absorption exhibits strong anisotropy and an oxygen isotope effect [47]. The nature of the residual electronic background can be attributed to competing orders due to density wave correlations and fluctuations [15], and possibly a charge density wave within the CuO chains pinned by structural defects like oxygen vacancies [47].

The relationship between the in-gap electronic modes and superconductivity remains unclear and requires further research efforts outside the scope of the present study. In the following, we focus on the superconductivity-induced changes and examine the difference conductivity, $\Delta\sigma_1(\omega) = \sigma_1(\omega, T_{\text{low}}) - \sigma_1(\omega, T_{\text{high}})$, and difference permittivity, $\Delta\varepsilon_1(\omega) = \varepsilon_1(\omega, T_{\text{low}}) - \varepsilon_1(\omega, T_{\text{high}})$. Figure 3(a) shows the difference spectra for the 60 u.c. thick DyBCO film measured at $T_{\text{low}} = 7$ K compared to $T_{\text{high}} = T_c$. The majority of the changes occur below ~110 meV, indicated by the red arrow, consistent with results for near-optimally doped single crystal $YBa_2Cu_3O_{6.95}$ [48–51]. However, our accurate measurements also reveal a tail in the difference spectra that extends to energies as high as 0.6 eV [see the blue arrow in

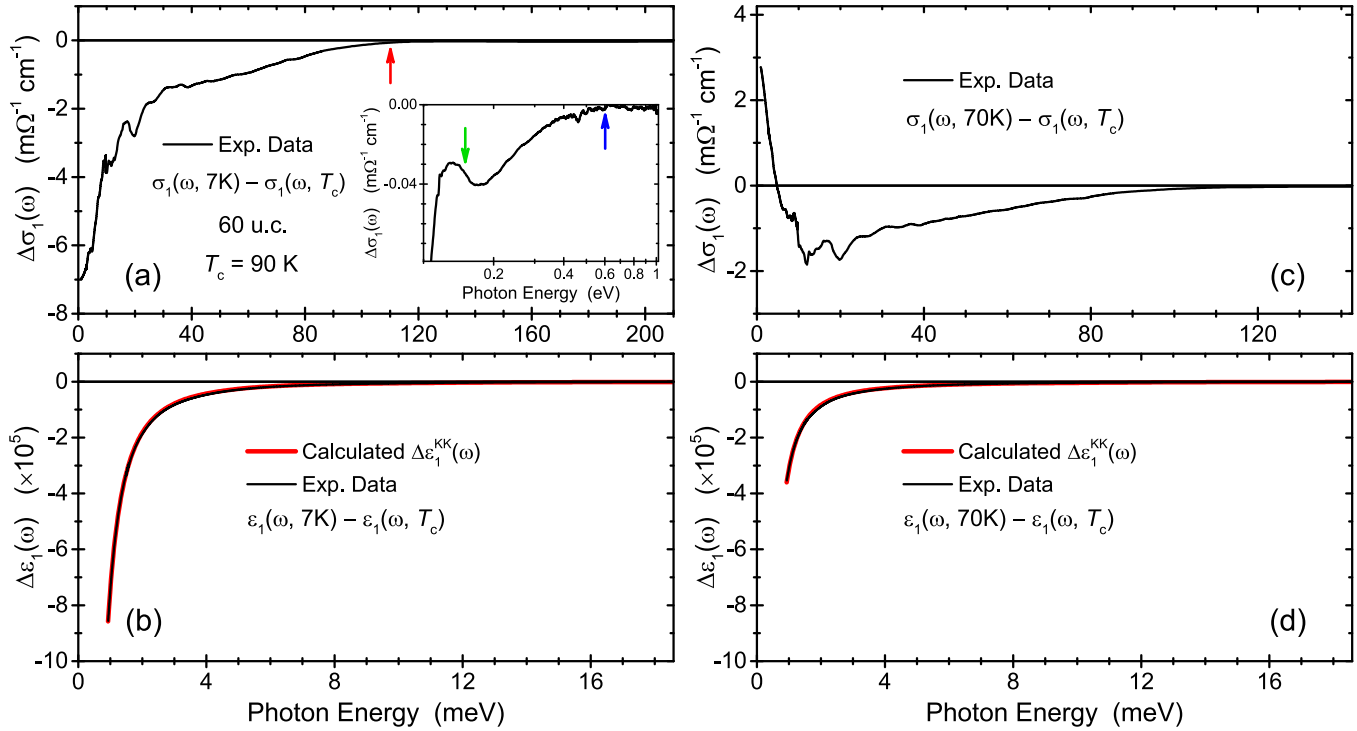

FIG. 3. The KK consistency analysis of the concomitant superconductivity-induced changes in the real parts of the optical conductivity and dielectric permittivity for a 60 u.c. thick DyBCO film with $T_c = 90$ K. The difference spectra, $\Delta\sigma_1(\omega) = \sigma_1(\omega, T_{\rm low}) - \sigma_1(\omega, T_{\rm high})$ and $\Delta\varepsilon_1(\omega) = \varepsilon_1(\omega, T_{\rm low}) - \varepsilon_1(\omega, T_{\rm high})$, account for the change in SW between (a), (b) 7 K and T_c and (c), (d) 70 K and T_c (black lines). The inset in panel (a) depicts the changes in the optical conductivity at higher energies extending up to 1 eV. Red, green, and blue arrows identify specific superconductivity-induced anomalies near 110 meV, 150 meV, and 0.6 eV, respectively. KK transformations of the $\Delta\sigma_1(\omega)$ extrapolations, as described in the main text, are plotted as red $\Delta\varepsilon_1^{\rm KK}(\omega)$ lines in (b) and (d), respectively, and agree with the experimentally measured black $\Delta\varepsilon_1(\omega)$ lines, indicating that the loss of intraband SW below T_c is equal to the weight of the superconducting δ function.

Fig. 3(a) inset]. While the superconductivity-induced changes in $\Delta\sigma_1(\omega)$ become two orders of magnitude smaller in this range, the integrated SW contained in the tail contributes ∼5% of the total SW transfer in the superconducting state. Remarkably, we find a weak but well-defined and reproducible feature at ∼150 meV, indicated by the green arrow in the Fig. 3(a) inset, which has also been observed in the superconductivity-induced response of $YBa_2Cu_3O_{6.9}$ single crystals [38]. The appearance of these three features below T_c is closely connected to the opening of the superconducting gap and boson-mediated coherence of Cooper pairs. Their characteristic energy scales are defined by the value and symmetry of the superconducting gap and specific features of the boson spectral function, providing a pathway to identify the pairing mechanism [8,12,52,53], as we discuss below in Sec. V B. To confirm that these energy scales are the only ones relevant to the pairing mechanism of superconductivity in DyBCO, it is necessary to compare the integrated SW loss below Ω_c to the strength of the δ function in the superconducting state.

The difference spectra $\Delta\sigma_1(\omega)$ and $\Delta\varepsilon_1(\omega)$ are directly connected through the KK relation,

$$\Delta\varepsilon_1(\omega) = 8\mathcal{P}\int_0^\infty \frac{\Delta\sigma_1(\omega')}{\omega'^2 - \omega^2}d\omega', \tag{2}$$

where $\mathcal{P}$ denotes the principal part. In our experimental approach both the real and imaginary parts of the dielectric function have been obtained independently, enabling us to use the KK relations to test for consistency of the measured data set. Since the FGT integral in Eq. (1) does not include the origin, Eq. (2) can be modified to explicitly include the contribution from the superconducting δ function:

$$\mathrm{SW}_1 = 8\int_{0^+}^\infty \Delta\sigma_1(\omega)d\omega, \tag{3}$$

$$\Delta\varepsilon_1^{\rm KK}(\omega) = 8\mathcal{P}\int_{0^+}^\infty \frac{\Delta\sigma_1(\omega')}{\omega'^2 - \omega^2}d\omega' - \frac{\mathrm{SW}_2}{\omega^2}. \tag{4}$$

Here, the SW loss SW_1 corresponds to the integrated difference conductivity spectra, while SW_2 is equivalent to ρ_s in Eq. (1). It is not possible to carry out experiments to truly zero or infinite frequency, so to perform the KK consistency analysis the measured $\Delta\sigma_1(\omega)$ data are extrapolated both to zero and infinity. One of the key strengths of our experimental approach is that it minimizes the extrapolation by measuring to energies as low as 0.8 meV and as high as 1.1 eV, where no changes in $\Delta\sigma_1(\omega)$ are detected within the noise level. Accordingly, the measured spectra are extrapolated above 1.1 eV with $\Delta\sigma_1(\omega) = 0$. We find that $\Delta\varepsilon_1^{\rm KK}(\omega)$, shown by the red curve in Fig. 3(b), agrees with the measured $\Delta\varepsilon_1(\omega)$ over a very broad energy range down to the lowest measured frequencies when $\mathrm{SW}_2 = -\mathrm{SW}_1$, implying that the total intraband SW is conserved and the FGT sum rule is obeyed. This agreement is strongly controlled by the amount of SW located at nonzero energies below ∼0.8 meV and not by the exact shape of the extrapolation.

Our approach also accounts for the low-energy response of thermally excited quasiparticles. To illustrate this, we apply the same numerical procedure to our data measured at intermediate temperatures, $T \approx \frac{3}{4}T_c$, where the order parameter changes rapidly and the normal fluid and superfluid terms give similar contributions to the optical conductivity $\tilde{\sigma}(\omega, T) = i\rho_n(T)/(\omega + i\gamma) + i\rho_s(T)/\omega$, with $\rho_n + \rho_s$ remaining constant. The experimental difference spectra and calculated $\Delta\varepsilon_1^{\mathrm{KK}}(\omega)$ for the 60 u.c. thick DyBCO film are displayed in Figs. 3(c) and 3(d) for spectra measured at $T_{\mathrm{low}} = 70$ K compared to $T_{\mathrm{high}} = T_c$. Steep positive changes in $\Delta\sigma_1(\omega)$ occur below ∼10−20 meV due to the temperature evolution of the low-energy quasiparticle peak [40]. This peak occurs as a result of competition between the decreasing quasiparticle scattering rate and decreasing normal charge carrier density as temperature is reduced in the superconducting state [54–56]. Comparing $\Delta\varepsilon_1^{\mathrm{KK}}(\omega)$ to the measured $\Delta\varepsilon_1(\omega)$, we find that the strength of the δ function, ρ_s, is equivalent to SW_1, confirming the FGT sum rule and two-fluid model are obeyed at intermediate temperatures. Equivalent results are obtained from the KK consistency analysis for the 20 u.c. thick DyBCO film, as shown in Figs. 9(a)–9(d) in the Appendix.

To quantify the degree of agreement between $\Delta\varepsilon_1^{\mathrm{KK}}(\omega)$ and $\Delta\varepsilon_1(\omega)$, we consider the dependence of the superfluid stiffness, $-\omega^2\Delta\varepsilon_1^{\mathrm{KK}}(\omega)$, on the amount of SW located in the low-energy extrapolation of $\Delta\sigma_1(\omega)$, as shown in Figs. 4(a) and 4(b). Here, we consider the full dependence of $-\omega^2\Delta\varepsilon_1^{\mathrm{KK}}(\omega)$ from the lowest measured energies up to the characteristic phonon frequencies, rather than simply the estimated value of the superfluid stiffness in the limit $\omega \to 0$ [51]. The accurate fit of $-\omega^2\Delta\varepsilon_1(\omega)$ requires a significant positive SW component below ∼0.5 meV, corresponding to a low-energy quasiparticle peak that survives at 7 K with a very small scattering rate on the order of 0.1 meV. The presence of this peak is confirmed by manually unbalancing SW_1 and SW_2 by ±2% of the weight of the superconducting δ function, which produces a shift of $-\omega^2\Delta\varepsilon_1^{\mathrm{KK}}(\omega)$ by an amount consistent with the magnitude of the low-energy error bar in the spectra merging procedure. This unbalancing strongly bounds the extrapolation of $\Delta\sigma_1(\omega)$ to within the gray shaded area in Fig. 4(a). Such a narrow conductivity response is consistent with the low-energy, cusp-like quasiparticle peak observed in gigahertz surface impedance measurements down to 1 K that arises from weak scattering of nodal quasiparticles [28,57]. Our approach allows us to account for this peak with high precision, in contrast to conventional infrared spectroscopy techniques where the KK relations cannot be used to independently check the consistency of the measured data. We find that the SW of the narrow quasiparticle peak constitutes as much as 6% of the SW of the δ function, which exceeds the accuracy of conventional spectroscopic methods [51].

The precision of our experimental technique can be further highlighted by placing the size of the error bar in terms of the total intraband charge carrier density, $\mathrm{SW}(T_c) = 8\int_{0^+}^{1.1\,\mathrm{eV}} \sigma_1(\omega, T_c)d\omega$. By comparing the 2% uncertainty in the balance of SW between the superconducting δ function and the narrow quasiparticle peak to the absolute (undif-

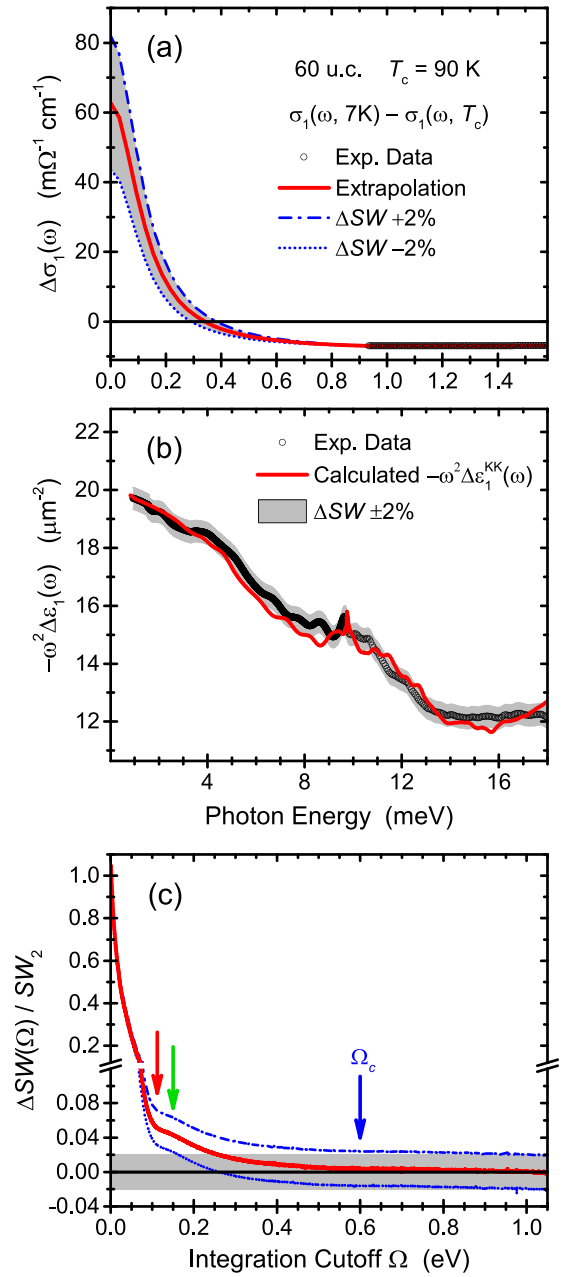

FIG. 4. (a), (b) An analysis of the accuracy of the KK consistency procedure, focusing on the extreme low-frequency portion of the measured spectrum. The solid red lines represent (a) the low-energy extrapolation of $\Delta\sigma_1(\omega)$ and (b) its associated KK transform in terms of the superfluid stiffness $-\omega^2\Delta\varepsilon_1^{\mathrm{KK}}(\omega)$, which best matches the measured $-\omega^2\Delta\varepsilon_1(\omega)$ data (black circles). The two blue dash-dotted curves represent the same KK analysis with the SW contained in the superconducting δ function unbalanced (increased and decreased) by 2%. (c) The integrated gain of intraband SW between 7 K and T_c, defined by Eq. (5), as a function of the upper integration bound Ω. Within the experimental error bar (shown by the gray shaded area and blue dash-dotted curves), the shift of SW between superconducting and quasiparticle components is fully balanced by integrating up to $\Omega \approx 0.6$ eV. The red, green, and blue arrows indicate the positions of the specific spectral anomalies highlighted in Fig. 3(a).

ferenced) SW in the normal state, we find that $(SW_1 + SW_2)/SW(T_c) \approx \pm 0.2\%$. From $SW(T_c) = 4.16\ eV^2$, this implies the FGT sum rule is valid to within $\pm 0.01\ eV^2$.

With the accurate frequency dependence of $\Delta\sigma_1(\omega)$ from zero to 1.1 eV determined, we obtain the energy bound Ω_c required to fully recover the SW that has shifted into the δ function in the superconducting state. Figure 4(c) depicts the recovery of the total intraband SW as a function of the integration cutoff Ω,

$$\Delta SW(\Omega) = 8 \int_{0^+}^{\Omega} \Delta\sigma_1(\omega) d\omega + SW_2. \quad (5)$$

Within the error bar, the total intraband SW is recovered up to $\Omega_c \approx 0.6$ eV, and the uncertainty in the low-energy extrapolation produces only a very small vertical shift in the recovered SW. A large range of frequencies where $\Delta SW(\Omega) = 0$ extends from $\Omega \approx 0.6$ eV to beyond 1 eV, above the measured spectral range, demonstrating that the SW shift responsible for the formation of the superconducting condensate is well separated from interband contributions to the optical conductivity. In comparison, previously reported results based on infrared reflectivity measurements [51] indicated that the superfluid density ρ_s in optimally doped $YBa_2Cu_3O_{6.95}$ single crystals is recovered to within ~5% of its SW up to ~0.1 eV, in good agreement with our observation that the majority (~95%) of the changes in $\Delta\sigma_1(\omega)$ occur below ~110 meV [red arrow in Fig. 4(c)]. The improved accuracy of our measurements allowed us to resolve the tail in $\Delta\sigma_1(\omega)$ that extends up to ~0.6 eV.

IV. NORMAL STATE CHARGE CARRIER SW

While the total intraband SW remains constant for temperatures $T < T_c$, different behavior is observed above T_c. To follow the temperature dependence of the intraband SW in our DyBCO films, we perform KK consistency analyses above T_c for difference spectra $\Delta\sigma_1(\omega)$ and $\Delta\varepsilon_1(\omega)$ with $T_{low} = T_c$. The measured difference spectra are found to be KK consistent within the error bar of the experiment without any contribution from a δ-function component or sharp accumulation of SW below ~1 meV, as illustrated in Fig. 5 for the 60 u.c. thick film and Figs. 9(e) and 9(f) for the 20 u.c. thick film (see the Appendix). The result depends only on the narrowing of the broad Drude-like component below ~30–40 meV. For both films we find that the value of the integrated difference SW is positive, with $\Delta SW/SW(T_c) \approx 2\%$ between 200 K and T_c, in agreement with the prior reported experimental data for cuprates [21,22,51]. Indeed, for several families of underdoped, optimally doped, and overdoped cuprates the total intraband SW has been observed to follow a T^2 dependence with an increase on the order of $\Delta SW/SW(T_c) \approx 3$–5% between 300 K and the superconducting state when the integral in Eq. (5) is taken to $\Omega \approx 1$ eV [4,58]. Over a broad temperature range the total intraband SW changes due to smearing of the Fermi occupation function around the Fermi level with increasing temperature. In a tight-binding picture, $SW(T) = SW_0 - kT^2$ so that the total intraband SW increases with decreasing temperature as less of the Fermi function tail lies at high energies corresponding to interband transitions [59]. This

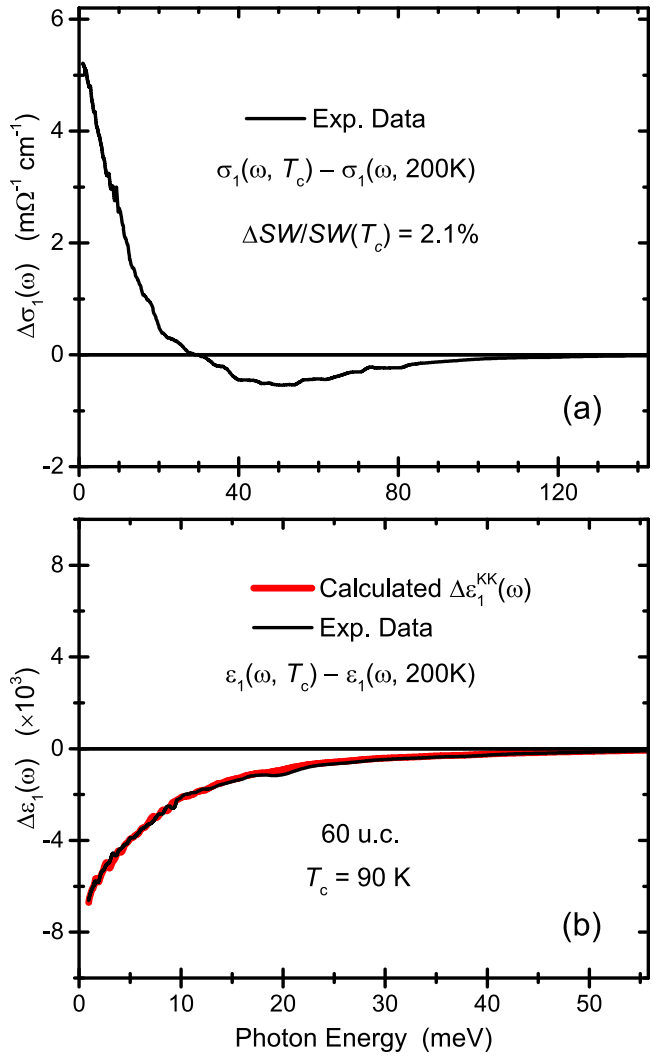

FIG. 5. The KK consistency analysis of the concomitant changes in $\Delta\sigma_1(\omega)$ and $\Delta\varepsilon_1(\omega)$ (black lines) for a 60 u.c. thick DyBCO film above $T_c = 90$ K. The extrapolated $\Delta\sigma_1(\omega)$ curve and its calculated KK transformation are given by the red lines in (a) and (b), respectively. SW accumulated at low frequencies between T_c and 200 K in (a) accounts for an increase of the total quasiparticle SW by $[SW(T_c) - SW(200\ K)]/SW(T_c) = 2.1\%$.

increase is consistent with plaquette dynamical mean-field theory calculations [60] in the framework of the t-J model where the increase in total intraband SW of 3–5% between 300 K and T_c was found to be doping independent.

V. DISCUSSION

A. Temperature evolution of quasiparticle SW

Figure 6 depicts the temperature dependence of the total intraband SW in the 60 u.c. thick DyBCO film, $SW(T) = 8\int_{0^+}^{1.1\ eV} \sigma_1(\omega, T) d\omega$, normalized to its value at T_c. $SW(T)$ remains constant within the 0.2% error bar at $T < T_c$ while $SW(T) \propto T^2$ is observed above the superconducting transition. For a layered system such as the cuprates, the coefficient on T^2 can be expressed as $k = 2E_cB$ in the nearest-neighbor tight-binding approximation [4,59], where the charging energy $E_c = 2\pi e^2/d$, B is a factor inversely

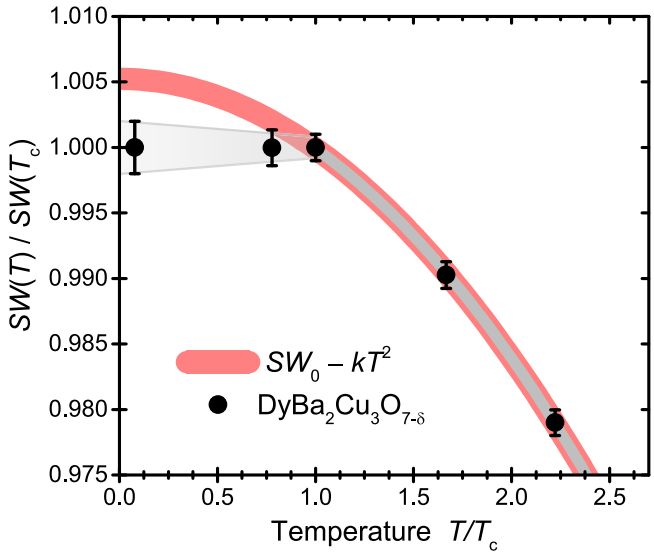

FIG. 6. The total intraband SW of the 60 u.c. thick DyBCO film as a function of reduced temperature, normalized to its value at T_c. Above T_c the quasiparticle SW follows the quadratic dependence $\mathrm{SW}(T) = \mathrm{SW}_0 - kT^2$ (red shaded line). Below T_c the total intraband SW remains constant to within the error bar. At the lowest measured temperature of 7 K this constitutes a superconductivity-induced reduction of intraband SW of ∼0.5% compared to the normal state single-band value.

proportional to the bandwidth, and d is the spacing between adjacent CuO_2 planes (≈6 Å for DyBCO). From a fit of the above-T_c data, shown by the thick red shaded line in Fig. 6, we obtain a value of $B = 9.3\ \mathrm{eV}^{-1}$. Extrapolation of the red shaded line to $T \to 0$ indicates an overshoot of $\mathrm{SW}(T)/\mathrm{SW}(T_c)$ by ∼0.5% above its measured value in the superconducting state, corresponding to a superconductivity-induced SW supression of $-0.02\ \mathrm{eV}^2$ at 7 K. Since the total intraband SW in the tight-binding approximation may also be identified with the negative expectation value of the kinetic energy K per in-plane Cu atom, $\int_{0^+}^{1.1\,\mathrm{eV}} \sigma_1(\omega)d\omega \sim E_c\langle -K\rangle$ [61], we equate the plasma frequency $\omega_p \equiv \sqrt{\mathrm{SW}(T_c)} = 2.04$ eV to $\langle K\rangle = 277$ meV/Cu and the superconductivity-induced reduction of intraband SW to a small kinetic energy increase of $\Delta\langle -K\rangle = 1.5 \pm 0.6$ meV/Cu. The precise validity of the FGT sum rule and slight increase of in-plane kinetic energy in the superconducting state of our DyBCO films rules out unusual kinetic energy saving pairing mechanisms [17,18] as the primary driver of superconductivity in optimally doped *R*BCO cuprates. These results are in agreement with previously reported measurements on $YBa_2Cu_3O_{6.9}$ single crystals [38]. The measured increase in $\langle K\rangle$ is comparable to but smaller than the gain in magnetic exchange energy of ∼2 meV/Cu that is available to the superconducting condensation energy, which is in fact an order of magnitude smaller [62].

B. Signatures of spin fluctuations

By applying a KK consistency analysis to the measured spectra, we find that the FGT sum rule is obeyed over energies extending up to $\Omega_c \approx 0.6$ eV, which lies beyond the energy scale expected for conventional phonon-mediated superconductivity [8,12]. The development of the theory of phonon-mediated superconductivity within the regime of strong electron-phonon coupling holds the potential to broaden the range of involved energies to include the characteristic polaron binding energies [63]. However, despite recent theoretical advancements [64,65], very little experimental evidence currently supports the idea that strong electron-phonon coupling governs the physics of cuprates beyond the undoped and weakly doped regimes.

Antiferromagnetic spin fluctuations have been established to play an essential role in the pairing physics of the cuprate HTSCs [15], where a clear correlation is observed between the spin-fluctuation spectrum measured by inelastic neutron scattering and the self-energy effects seen in angle-resolved photoemission spectroscopy [66]. In analogy to the case of phonon-mediated superconductors, this spin-fluctuation spectrum would form the basis for the electron-boson spectral function, $I^2\langle\chi_2(\omega)\rangle$, where I^2 is the coupling strength to the charge carriers. In the normal state, the spin-fluctuation spectrum is composed of paramagnon excitations that emanate from the wave vector $\vec{q} = (\pi, \pi)$, which characterizes antiferromagnetic order in undoped cuprates, and disperse up to ∼300 meV. The paramagnons are heavily damped such that the corresponding spectral features acquire a half-width-at-half-maximum of ∼200 meV. The full paramagnon spectrum thus extends up to $\Omega_{\mathrm{para}} \sim 600$ meV [16]. Less pronounced feedback effects of Cooper pairing on the magnetic fluctuation spectrum are also observed at energies far above the superconducting gap up to the magnetic zone boundary [67]. The broad continuum in the difference conductivity extending up to $\Omega_c \approx 0.6$ eV can therefore be attributed to scattering from damped spin excitations, where $\Omega_c \sim 2\Delta_{\mathrm{max}} + \Omega_{\mathrm{para}}$ (here Δ_{max} is the maximum of the d-wave superconducting gap) [68–70].

The concept of spin-fluctuation mediated pairing is further supported by the presence of two additional anomalies in the difference conductivity at lower energies, as indicated by the red and green colored arrows in Figs. 3(a) and 4(c). In the superconducting state, an intense resonant mode develops at $\Omega_s = 41$ meV at $\vec{q} = (\pi, \pi)$ [71]. The specific form and manifestation of the superconductivity-induced anomalies in the optical conductivity, within the framework of the spin-fermion model, strongly rely on assumptions about the collective boson momentum dispersion, the d-wave superconducting gap structure, and the degree of impurity scattering. The feature in the difference conductivity near 150 meV, marked by the green arrow in Fig. 3(a), is in excellent agreement with the weak singularity expected in $\sigma_1(\omega)$ at $2\Delta_{\mathrm{max}} + 2\Omega_s$ [53,70], with the maximum of the d-wave superconducting gap at $2\Delta_{\mathrm{max}} \approx 65$ meV deduced by electronic Raman scattering in $YBa_2Cu_3O_{6.95}$ and the sharp resonance mode at $\Omega_s < 2\Delta_{\mathrm{max}}$ [71]. Under the conditions of strong impurity scattering in the dirty limit, the major superconductivity-induced changes are found to primarily occur within the 2Δ region and do not exhibit prominent manifestations at 4Δ. Within this approach, the characteristic frequency near 110 meV for the main changes in $\Delta\sigma_1(\omega)$ [red arrow in Fig. 3(a)] can be reasonably assigned as $2\Delta_{\mathrm{max}} + \Omega_s$ [53,70] due to the onset of scattering from the boson mode.

Notably, the functional form of theoretical calculations for $\Delta SW(\Omega)/SW(T_c)$ in Figs. 10 and 11 in Ref. [70], based on a spin-fluctuation collective-boson model taking into account lattice interactions, agrees well with our experimental result in Fig. 4(c). This scenario is also consistent with recent scanning tunneling experiments showing that superexchange interactions, which set the exchange coupling J, control the strength of the superconducting condensate density [72]. Indeed, cluster dynamical mean field theory calculations derived from a fluctuation-diagnostics approach extended to the d-wave superconducting state of the two-dimensional Hubbard model have identified antiferromagnetic spin fluctuations as the dominant source of pairing in cuprates, albeit with a more complex structure than those typically considered in standard spin fluctuation theories [73].

Central to the issue of the FGT sum rule and spin fluctuations in cuprate HTSCs is the dependence of these properties on hole doping. Our results for near-optimally doped DyBCO films agree with prior reported measurements of the SW transfer in optimally doped YBCO single crystals [38]. However, previously reported results for different doping levels and other cuprate families are widely divergent [21,35,51]. In particular, far-infrared reflectivity measurements in $Bi_2Sr_2CaCu_2O_{8+\delta}$ [34,36] have suggested that integrated SW increases below T_c on the underdoped side of the phase diagram and decreases in the overdoped regime, with a crossover near optimal doping. In contrast, other infrared reflectivity measurements in underdoped $YBa_2Cu_3O_{6.60}$ [51] found that the FGT sum rule is satisfied at $\Omega_c \sim 0.6$ eV, in full agreement with our data on near-optimally doped DyBCO. It is expected within the framework of the collective spin-fluctuation theory that the relative changes in $\Delta\sigma_1(\omega)$ above $2\Delta_{\max} + \Omega_s$ are more pronounced in the underdoped regime due to the reduced charge carrier density and decreased damping of the paramagnon by a larger value of $2\Delta_{\max}$ [16,71]. This makes an experimental approach based on the reflectivity technique sufficient to uncover the superconductivity-induced optical anomalies in underdoped single crystals, whereas our measurements require thin films. We find that underdoped DyBCO thin films do not maintain a stable doping level on the timescale of this experiment. Resonant inelastic x-ray scattering experiments show that the cutoff of the collective spin-fluctuation spectrum is largely independent of doping [74,75], but that it increases from one cuprate family to the next in proportion to the number of CuO_2 layers per unit cell and maximum T_c [76]. Beyond optimal doping the paramagnon spectrum exhibits a sharp crossover from a regime defined by collective spin excitations to one dominated by incoherent particle-hole excitations [77]. It is possible that these findings may elucidate the similarity between the observations reported for optimally doped and underdoped *R*BCO [38,51], and the differences between *R*BCO and $Bi_2Sr_2CaCu_2O_{8+\delta}$ [34,36].

It cannot yet be ruled out that the differences in the published optical data arise from differences in analysis, especially those arising from systematic offsets in the recovered SW due to the specific treatment of low-frequency data in far-infrared reflectivity experiments. The experimental method we have presented here, based on fully phase-sensitive measurements of the complex dielectric function from less than

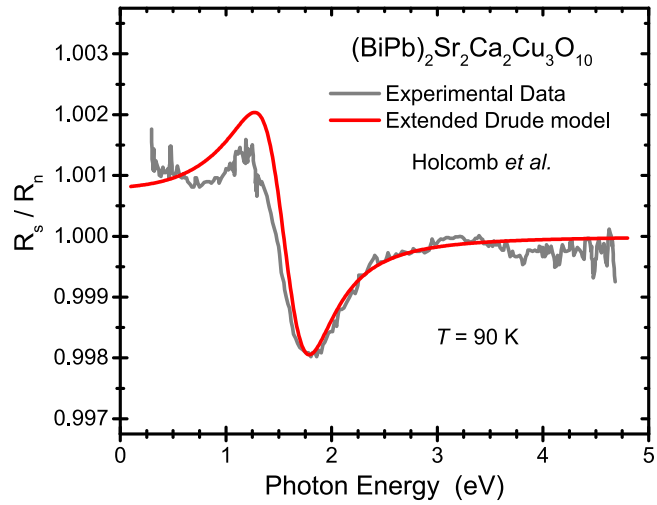

FIG. 7. The superconducting-to-normal state reflectance ratio, R_s/R_n, for a c-axis-oriented $(BiPb)_2Ba_2Ca_2Cu_3O_{10}$ thin film (gray line) [19]. The structure in the vicinity of the plasma edge can be captured by considering an extended Drude model, $\tilde{\varepsilon}(\omega, T) = \varepsilon_\infty - \omega_p^2/[\omega^2 - i\omega\gamma(\omega, T)]$, where the quasiparticle scattering rate $\gamma(\omega, T) = A(k_B T)^2 + B\omega$. The red line represents an extended Drude model fit using the parameters given in Ref. [19], with ω_p remaining constant across the transition. The structure in R_s/R_n near the plasma edge reflects a small narrowing of the quasiparticle peak below T_c by $\Delta\gamma/\gamma_n \approx 0.2\%$.

1 meV to above 1 eV, provides a robust way to control the balance of SW between the superconducting and quasiparticle contributions to the optical conductivity. Measurements following the procedure we have outlined here will need to be carried out at other doping levels and in other cuprate families to clarify this issue, with the results compared to doping- and material-dependent studies of various collective excitations.

C. SW redistribution beyond Ω_c

Our observation that the total intraband SW is recovered up to $\Omega_c \approx 0.6$ eV within $\pm 0.2\%$ implies that superconductivity-induced anomalies observed beyond Ω_c reflect either minor (within 0.2%) or no effect on the quasiparticle SW. The trend below T_c shown in Fig. 6, therefore, remains unaffected by any redistribution of SW at high energies. Nonetheless, we comment on prior observations and possible mechanisms for such anomalies for completeness.

To date, the reported optical anomalies at high energies primarily occur at or near the plasma edge [19,21,22,24,32–38]. In cuprate HTSCs the scattering rate is quite large, and its change across T_c causes variations in the optical conductivity up to the plasma edge at about 1.5 eV, corresponding to the peak in the loss function. SW removed from the high-energy Drude tail is transferred to the "head" of the Drude peak near the origin, leaving the total intraband SW unaffected. The changes in the optical conductivity in the Drude tail above 0.6 eV are within the noise level of Fig. 3, but may nevertheless be detected in the corresponding shift of the plasma edge. In particular, as illustrated in Fig. 7, the blue shift of the superconductivity-induced thermal-modulation reflectivity near the plasma edge [19] can be captured by considering a

minor narrowing of the quasiparticle peak below T_c while the plasma frequency remains constant. The drop in the inelastic scattering rate below T_c is also evident from a peak in σ_1 versus temperature that is observed in the microwave-to-terahertz conductivity upon the opening of the superconducting gap [28,40,54–57]. The observed changes in $\gamma(\omega)$ have been addressed by the contribution of spin-fluctuation scattering processes to the quasiparticle lifetime [27].

Superconductivity-induced anomalies in the optical conductivity may even occur above the plasma edge at energies corresponding to interband transitions, as detected in the multiband pnictide superconductor $Ba_{0.68}K_{0.32}Fe_2As_2$ [78]. In multiband HTSCs, redistribution of the occupation of the bands below T_c can be generated by imbalanced lowering of the chemical potential in bands with different superconducting gap energies,

$$\frac{\Delta\mu_j}{\mu_0} = \frac{1}{4}\left(\frac{\Delta_j}{\mu_0}\right)^2\left(\ln\frac{2\Omega_D}{\Delta_j} - 1\right), \tag{6}$$

with Ω_D an energy of order several times the Debye energy in phonon-mediated superconductors [79,80]. This effect, albeit quite small in conventional superconductors, may become essential in the presence of a high density of states near the Fermi level caused by a van Hove singularity [81]. In this scenario, depicted in Fig. 8, the total quasiparticle SW is not necessarily affected. A similar effect was also considered for cuprate superconductors by taking into account their multiorbital character [82]. The high-energy optical anomalies in multiorbital systems have also recently been discussed in terms of the nontrivial quantum geometry of the conduction band [29–31], but the detailed relationship between quantum geometry and SW is complicated by orbital-dependent pairing and it remains difficult to quantify how changes in the spectrum at high energies are related to the superfluid density.

VI. CONCLUSION

In summary, we report high-precision measurements of the FGT sum rule and optical conductivity SW transfer across T_c in near-optimally doped $DyBa_2Cu_3O_{7-\delta}$ thin films. In our approach, we combine submillimeter-microwave interferometry, high-resolution terahertz time-domain spectroscopy, and infrared spectroscopic ellipsometry to obtain fully phase-sensitive measurements of the real and imaginary parts of the complex dielectric function between 0.8 meV and 1.1 eV. The FGT sum rule is then examined by performing a KK consistency analysis on the independently measured $\Delta\sigma_1(\omega)$ and $\Delta\varepsilon_1(\omega)$ data. We find that the FGT sum rule is satisfied with an unprecedented accuracy of $\pm 2\%$, leaving the total intraband SW unchanged in the superconducting state with an accuracy of $\pm 0.2\%$, with a cutoff of $\Omega_c \approx 0.6$ eV. Tracking the balance of SW from 7 to 200 K suggests that the in-plane kinetic energy $\langle K\rangle$ increases by 1.5 ± 0.6 meV/Cu in the superconducting state, ruling out possible kinetic energy saving pairing mechanisms in near-optimally doped *R*BCO cuprates.

Additionally, we observe specific anomalies in the measured $\Delta\sigma_1(\omega)$ spectra below T_c near 110 and 150 meV, which we assign as $2\Delta_{\max} + \Omega_s$ and $2\Delta_{\max} + 2\Omega_s$, respectively. In the framework of antiferromagnetic spin-fluctuation theory [52,53], $2\Delta_{\max}$ corresponds to twice the maximum of the

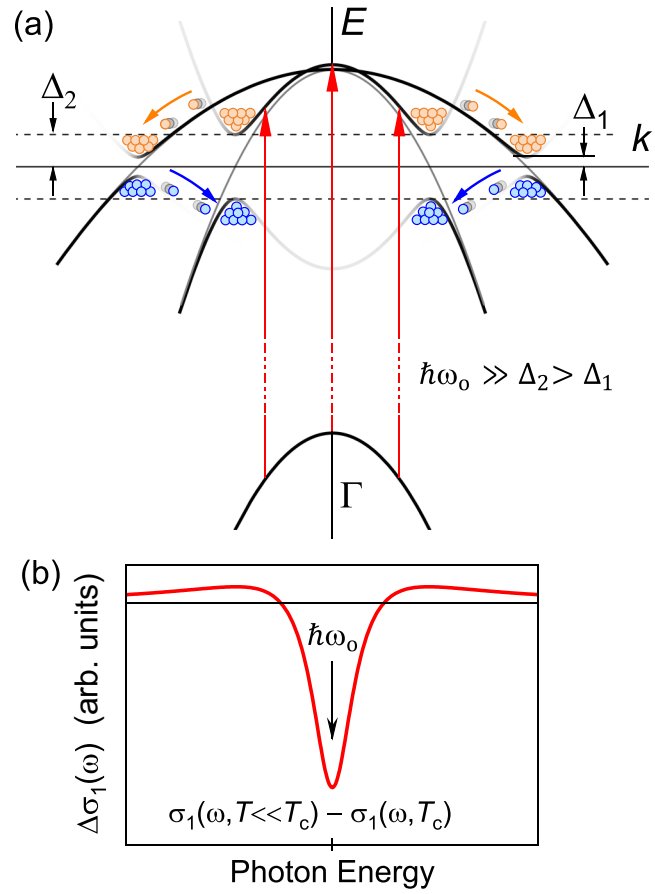

FIG. 8. (a) A schematic representation of the band structure of a two-band superconductor in the normal (thin solid parabolas) and superconducting (thick black and gray Bogoliubov dispersions) states, after Ref. [78]. Redistribution of the occupation of the different bands below T_c is caused by imbalanced lowering of the chemical potential in bands with different superconducting gap energies, $\Delta\mu_{1,2}/\mu_0 \approx (\Delta_{1,2}/2\mu_0)^2$, as shown by the orange and blue arrows for holes and electrons, respectively. This redistribution causes the depletion (increase) of unoccupied states in the narrow (broad) parabola. (b) The resulting difference of the real part of the optical conductivity between the superconducting and normal regimes for representative interband transitions shown by the red vertical arrows in panel (a). The total optical conductivity SW remains conserved.

d-wave superconducting gap, $2\Delta_{\max} \approx 65$ meV, and $\Omega_s = 41$ meV is identified as the sharp resonance mode observed in inelastic neutron scattering [71]. Furthermore, the cutoff of the FGT sum rule, $\Omega_c \approx 0.6$ eV, aligns with an absorption threshold in $\Delta\sigma_1(\omega)$ that is consistent with the cutoff of scattering from the spectrum of damped paramagnons [16]. The coupling of characteristic spin-fluctuation energy scales appearing in $\Delta\sigma_1(\omega)$ to the FGT sum rule is compatible with a picture of antiferromagnetic spin fluctuations as the dominant pairing mechanism in the *R*BCO family of cuprates. Further studies across different doping levels and compounds are imperative to draw general conclusions about the pairing mechanism in cuprate HTSCs. Taking advantage of the method outlined in this study will help to clarify the behavior of the FGT sum rule throughout the phase diagram.

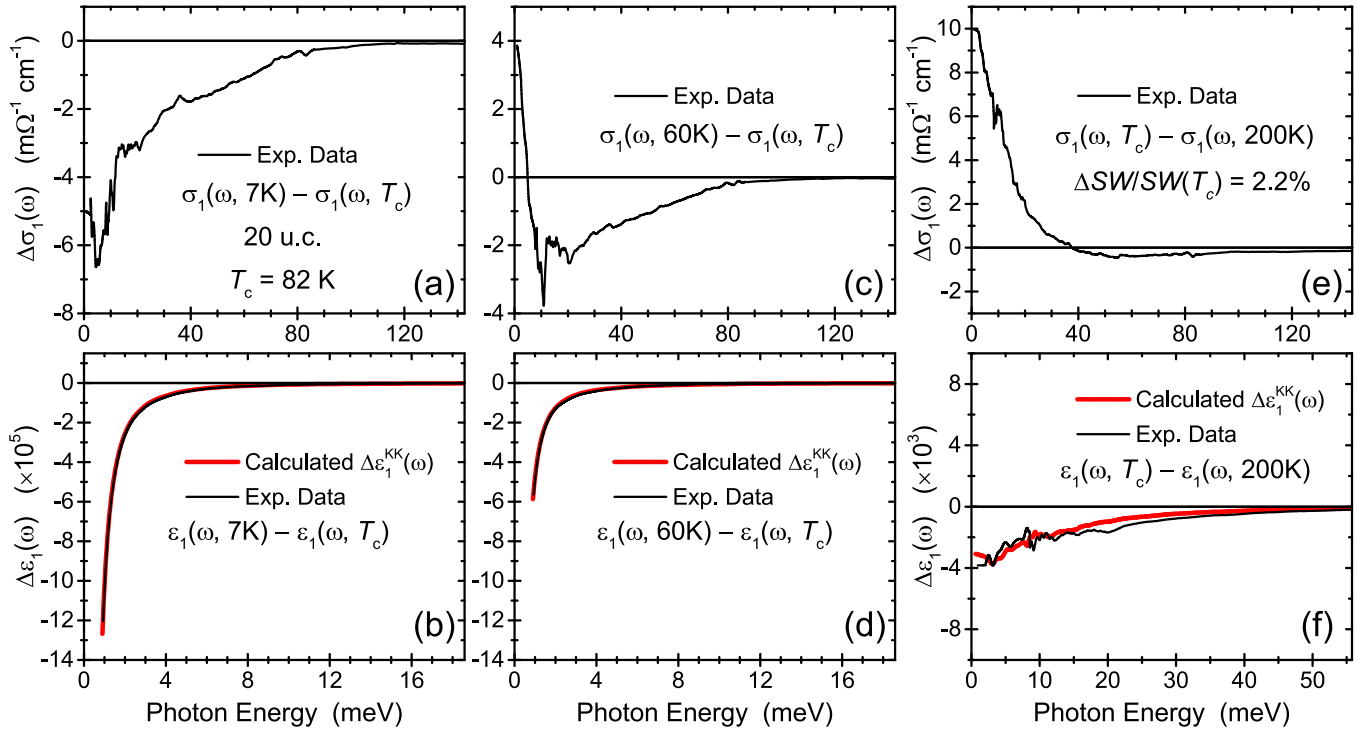

FIG. 9. The KK consistency analysis of the measured real parts of the optical conductivity and dielectric function for a 20 u.c. thick DyBCO film with $T_c = 82$ K. As in Fig. 3, the difference of the response functions, $\Delta\sigma_1(\omega)$ and $\Delta\varepsilon_1(\omega)$, were measured between (a), (b) 7 K and T_c, (c), (d) 60 K and T_c, and (e), (f) T_c and 200 K (black lines). The KK transformations of these extrapolations are plotted as the red lines in panels (b), (d), and (f), respectively. The calculated transforms agree with the measured data deep in the superconducting state (b), at intermediate temperatures closer to T_c (d) where a narrow quasiparticle peak is observed, and above T_c (f). Additionally, the SW accumulated below ~40 meV in panel (e) accounts for an increase of the intraband SW by 2.2% compared to its value at T_c, while, as in the case of the 60 u.c. thick DyBCO film, the total intraband SW remains constant below T_c.

ACKNOWLEDGMENT

R.D.D. thanks M. Minola and L. Del Re for fruitful discussions.

APPENDIX

We performed a KK consistency analysis on spectra measured both below and above $T_c = 82$ K in a near-optimally doped 20 u.c. thick DyBCO film, selected from the set used in Ref. [40]. Compared to the near-optimally doped 60 u.c. thick film, this thinner sample is characterized by larger tetragonal distortions due to the LSAT substrate and less quasiparticle scattering [39,40]. As can be seen in Figs. 9(a)–9(d), the FGT sum rule is found to be satisfied both deep in the superconducting state, at $T = 7$ K, and at intermediate temperatures, where the superconducting order parameter changes rapidly, exhibiting the same characteristic energy scales. Figures 9(e) and 9(f) depict the KK consistency analysis for the 20 u.c. thick DyBCO film in the normal state, as in Fig. 5. The total intraband SW increases by $\Delta\mathrm{SW}/\mathrm{SW}(T_c) \approx 2\%$ between 200 K and T_c.

[1] R. Kubo, J. Phys. Soc. Jpn. **12**, 570 (1957).
[2] M. Tinkham, *Introduction to Superconductivity*, 2nd ed. (Dover, Mineola, NY, 2004)
[3] D. N. Basov and T. Timusk, Rev. Mod. Phys. **77**, 721 (2005).
[4] L. Benfatto and S. G. Sharapov, Low Temp. Phys. **32**, 533 (2006).
[5] R. A. Ferrell and R. E. Glover, Phys. Rev. **109**, 1398 (1958).
[6] M. Tinkham and R. A. Ferrell, Phys. Rev. Lett. **2**, 331 (1959).
[7] S. B. Nam, Phys. Rev. **156**, 470 (1967).
[8] S. B. Nam, Phys. Rev. **156**, 487 (1967).
[9] G. M. Eliashberg, Zh. Eksp. Teor. Fiz. **38**, 966 (1960) [Sov. Phys. JETP **11**, 696 (1960)].
[10] A. Charnukha, O. V. Dolgov, A. A. Golubov, Y. Matiks, D. L. Sun, C. T. Lin, B. Keimer, and A. V. Boris, Phys. Rev. B **84**, 174511 (2011).
[11] R. R. Joyce and P. L. Richards, Phys. Rev. Lett. **24**, 1007 (1970).
[12] P. B. Allen, Phys. Rev. B **3**, 305 (1971).
[13] B. Farnworth and T. Timusk, Phys. Rev. B **10**, 2799 (1974).
[14] P. W. Anderson, Science **316**, 1705 (2007).
[15] B. Keimer, S. A. Kivelson, M. R. Norman, S. Uchida, and J. Zaanen, Nature (London) **518**, 179 (2015).

[16] M. Le Tacon, G. Ghiringhelli, J. Chaloupka, M. M. Sala, V. Hinkov, M. W. Haverkort, M. Minola, M. Bakr, K. J. Zhou, S. Blanco-Canosa, C. Monney, Y. T. Song, G. L. Sun, C. T. Lin, G. M. De Luca, M. Salluzzo, G. Khaliullin, T. Schmitt, L. Braicovich, and B. Keimer, Nat. Phys. **7**, 725 (2011).

[17] J. E. Hirsch, Physica C: Superconductivity **199**, 305 (1992).

[18] J. E. Hirsch and F. Marsiglio, Phys. Rev. B **62**, 15131 (2000).

[19] M. J. Holcomb, C. L. Perry, J. P. Collman, and W. A. Little, Phys. Rev. B **53**, 6734 (1996).

[20] A. J. Leggett, Proc. Natl. Acad. Sci. USA **96**, 8365 (1999).

[21] H. J. A. Molegraaf, C. Presura, D. van der Marel, P. H. Kes, and M. Li, Science **295**, 2239 (2002).

[22] A. F. Santander-Syro, R. P. S. M. Lobo, N. Bontemps, Z. Konstantinovic, Z. Z. Li, and H. Raffy, Europhys. Lett. **62**, 568 (2003).

[23] M. R. Norman, A. V. Chubukov, E. Van Heumen, A. B. Kuzmenko, and D. van der Marel, Phys. Rev. B **76**, 220509(R) (2007).

[24] J. Levallois, M. K. Tran, D. Pouliot, C. N. Presura, L. H. Greene, J. N. Eckstein, J. Uccelli, E. Giannini, G. D. Gu, A. J. Leggett, and D. van der Marel, Phys. Rev. X **6**, 031027 (2016).

[25] P. W. Phillips, L. Yeo, and E. W. Huang, Nat. Phys. **16**, 1175 (2020).

[26] X. Dong, E. Gull, and A. J. Millis, Nat. Phys. **18**, 1293 (2022).

[27] D. Duffy, P. J. Hirschfeld, and D. J. Scalapino, Phys. Rev. B **64**, 224522 (2001).

[28] P. J. Turner, R. Harris, S. Kamal, M. E. Hayden, D. M. Broun, D. C. Morgan, A. Hosseini, P. Dosanjh, G. K. Mullins, J. S. Preston, R. Liang, D. A. Bonn, and W. N. Hardy, Phys. Rev. Lett. **90**, 237005 (2003).

[29] L. Liang, T. I. Vanhala, S. Peotta, T. Siro, A. Harju, and P. Törmä, Phys. Rev. B **95**, 024515 (2017).

[30] J. Ahn and N. Nagaosa, Phys. Rev. B **104**, L100501 (2021).

[31] W. Chen and W. Huang, Phys. Rev. Res. **3**, L042018 (2021).

[32] A. B. Kuzmenko, H. J. A. Molegraaf, F. Carbone, and D. van der Marel, Phys. Rev. B **72**, 144503 (2005).

[33] N. Gedik, M. Langner, J. Orenstein, S. Ono, Y. Abe, and Y. Ando, Phys. Rev. Lett. **95**, 117005 (2005).

[34] G. Deutscher, A. F. Santander-Syro, and N. Bontemps, Phys. Rev. B **72**, 092504 (2005).

[35] F. Carbone, A. B. Kuzmenko, H. J. A. Molegraaf, E. van Heumen, E. Giannini, and D. van der Marel, Phys. Rev. B **74**, 024502 (2006).

[36] F. Carbone, A. B. Kuzmenko, H. J. A. Molegraaf, E. Van Heumen, V. Lukovac, F. Marsiglio, D. Van Der Marel, K. Haule, G. Kotliar, H. Berger, S. Courjault, P. H. Kes, and M. Li, Phys. Rev. B **74**, 064510 (2006).

[37] C. Giannetti, F. Cilento, S. D. Conte, G. Coslovich, G. Ferrini, H. Molegraaf, M. Raichle, R. Liang, H. Eisaki, M. Greven, A. Damascelli, D. van der Marel, and F. Parmigiani, Nat. Commun. **2**, 353 (2011).

[38] A. V. Boris, N. N. Kovaleva, O. V. Dolgov, T. Holden, C. T. Lin, B. Keimer, and C. Bernhard, Science **304**, 708 (2004).

[39] D. Putzky, P. Radhakrishnan, Y. Wang, P. Wochner, G. Christiani, M. Minola, P. A. van Aken, G. Logvenov, E. Benckiser, and B. Keimer, Appl. Phys. Lett. **117**, 072601 (2020).

[40] R. D. Dawson, K. S. Rabinovich, D. Putzky, G. Christiani, G. Logvenov, B. Keimer, and A. V. Boris, Phys. Rev. Lett. **125**, 237001 (2020).

[41] A. V. Boris, Y. Matiks, E. Benckiser, A. Frano, P. Popovich, V. Hinkov, P. Wochner, M. Castro-Colin, E. Detemple, V. K. Malik, C. Bernhard, T. Prokscha, A. Suter, Z. Salman, E. Morenzoni, G. Cristiani, H. U. Habermeier, and B. Keimer, Science **332**, 937 (2011).

[42] J. A. Woollam Co., Inc., *Guide to Using WVASE: Spectroscopic Ellipsometry Data Acquisition and Analysis Software* (J. A. Woollam Company, Lincoln, NE, 2012).

[43] G. Klatt, R. Gebs, C. Janke, T. Dekorsy, and A. Bartels, Opt. Express **17**, 22847 (2009).

[44] R. Gebs, G. Klatt, C. Janke, T. Dekorsy, and A. Bartels, Opt. Express **18**, 5974 (2010).

[45] G. Kozlov and A. Volkov, in *Millimeter and Submillimeter Wave Spectroscopy of Solids*, edited by G. Grüner (Springer-Verlag, Berlin, 1998), Chap. 3, pp. 51–109.

[46] B. Gorshunov, A. Volkov, I. Spektor, A. Prokhorov, A. Mukhin, M. Dressel, S. Uchida, and A. Loidl, Int. J. Infrared Millimeter Waves **26**, 1217 (2005).

[47] C. Bernhard, T. Holden, A. V. Boris, N. N. Kovaleva, A. V. Pimenov, J. Humlicek, C. Ulrich, C. T. Lin, and J. L. Tallon, Phys. Rev. B **69**, 052502 (2004).

[48] C. Bernhard, T. Holden, J. Humlıcek, D. Munzar, A. Golnik, M. Kläser, T. Wolf, L. Carr, C. Homes, B. Keimer, and M. Cardona, Solid State Commun. **121**, 93 (2002).

[49] D. N. Basov, R. Liang, D. A. Bonn, W. N. Hardy, B. Dabrowski, M. Quijada, D. B. Tanner, J. P. Rice, D. M. Ginsberg, and T. Timusk, Phys. Rev. Lett. **74**, 598 (1995).

[50] N. L. Wang, S. Tajima, A. I. Rykov, and K. Tomimoto, Phys. Rev. B **57**, R11081 (1998).

[51] C. C. Homes, S. V. Dordevic, D. A. Bonn, R. Liang, and W. N. Hardy, Phys. Rev. B **69**, 024514 (2004).

[52] J. P. Carbotte, E. Schachinger, and D. N. Basov, Nature (London) **401**, 354 (1999).

[53] A. Abanov, A. V. Chubukov, and J. Schmalian, Phys. Rev. B **63**, 180510(R) (2001).

[54] M. C. Nuss, P. M. Mankiewich, M. L. O'Malley, E. H. Westerwick, and P. B. Littlewood, Phys. Rev. Lett. **66**, 3305 (1991).

[55] D. A. Bonn, P. Dosanjh, R. Liang, and W. N. Hardy, Phys. Rev. Lett. **68**, 2390 (1992).

[56] F. Gao, G. L. Carr, C. D. Porter, D. B. Tanner, G. P. Williams, C. J. Hirschmugl, B. Dutta, X. D. Wu, and S. Etemad, Phys. Rev. B **54**, 700 (1996).

[57] A. Hosseini, R. Harris, S. Kamal, P. Dosanjh, J. Preston, R. Liang, W. N. Hardy, and D. A. Bonn, Phys. Rev. B **60**, 1349 (1999).

[58] A. Toschi, M. Capone, M. Ortolani, P. Calvani, S. Lupi, and C. Castellani, Phys. Rev. Lett. **95**, 097002 (2005).

[59] L. Benfatto, S. G. Sharapov, N. Andrenacci, and H. Beck, Phys. Rev. B **71**, 104511 (2005).

[60] K. Haule and G. Kotliar, Phys. Rev. B **76**, 104509 (2007).

[61] D. Baeriswyl, C. Gros, and T. M. Rice, Phys. Rev. B **35**, 8391 (1987).

[62] H. Woo, P. Dai, S. M. Hayden, H. A. Mook, T. Dahm, D. J. Scalapino, T. G. Perring, and F. Doğan, Nat. Phys. **2**, 600 (2006).

[63] A. S. Mishchenko, N. Nagaosa, Z.-X. Shen, G. De Filippis, V. Cataudella, T. P. Devereaux, C. Bernhard, K. W. Kim, and J. Zaanen, Phys. Rev. Lett. **100**, 166401 (2008).

[64] C. Zhang, J. Sous, D. R. Reichman, M. Berciu, A. J. Millis, N. V. Prokof'ev, and B. V. Svistunov, Phys. Rev. X **13**, 011010 (2023).
[65] A. S. Mishchenko, I. S. Tupitsyn, N. Nagaosa, and N. Prokof'ev, Sci. Rep. **11**, 9699 (2021).
[66] T. Dahm, V. Hinkov, S. V. Borisenko, A. A. Kordyuk, V. B. Zabolotnyy, J. Fink, B. Büchner, D. J. Scalapino, W. Hanke, and B. Keimer, Nat. Phys. **5**, 217 (2009).
[67] Y. Li, M. Le Tacon, M. Bakr, D. Terrade, D. Manske, R. Hackl, L. Ji, M. K. Chan, N. Barišić, X. Zhao, M. Greven, and B. Keimer, Phys. Rev. Lett. **108**, 227003 (2012).
[68] M. R. Norman and A. V. Chubukov, Phys. Rev. B **73**, 140501(R) (2006).
[69] J. Fink, A. Koitzsch, J. Geck, V. Zabolotnyy, M. Knupfer, B. Büchner, A. Chubukov, and H. Berger, Phys. Rev. B **74**, 165102 (2006).
[70] S. Maiti and A. V. Chubukov, Phys. Rev. B **81**, 245111 (2010).
[71] S. Pailhès, C. Ulrich, B. Fauqué, V. Hinkov, Y. Sidis, A. Ivanov, C. T. Lin, B. Keimer, and P. Bourges, Phys. Rev. Lett. **96**, 257001 (2006).
[72] S. M. O'Mahony, W. Ren, W. Chen, Y. X. Chong, X. Liu, H. Eisaki, S. Uchida, M. H. Hamidian, and J. C. Davis, Proc. Natl. Acad. Sci. USA **119**, e2207449119 (2022).
[73] X. Dong, L. Del Re, A. Toschi, and E. Gull, Proc. Natl. Acad. Sci. USA **119**, e2205048119 (2022).
[74] M. Le Tacon, M. Minola, D. C. Peets, M. M. Sala, S. Blanco-Canosa, V. Hinkov, R. Liang, D. A. Bonn, W. N. Hardy, C. T. Lin, T. Schmitt, L. Braicovich, G. Ghiringhelli, and B. Keimer, Phys. Rev. B **88**, 020501(R) (2013).
[75] M. Minola, G. Dellea, H. Gretarsson, Y. Y. Peng, Y. Lu, J. Porras, T. Loew, F. Yakhou, N. B. Brookes, Y. B. Huang, J. Pelliciari, T. Schmitt, G. Ghiringhelli, B. Keimer, L. Braicovich, and M. Le Tacon, Phys. Rev. Lett. **114**, 217003 (2015).
[76] L. Wang, G. He, Z. Yang, M. Garcia-Fernandez, A. Nag, K. Zhou, M. Minola, M. L. Tacon, B. Keimer, Y. Peng, and Y. Li, Nat. Commun. **13**, 3163 (2022).
[77] M. Minola, Y. Lu, Y. Y. Peng, G. Dellea, H. Gretarsson, M. W. Haverkort, Y. Ding, X. Sun, X. J. Zhou, D. C. Peets, L. Chauviere, P. Dosanjh, D. A. Bonn, R. Liang, A. Damascelli, M. Dantz, X. Lu, T. Schmitt, L. Braicovich, G. Ghiringhelli *et al.*, Phys. Rev. Lett. **119**, 097001 (2017).
[78] A. Charnukha, P. Popovich, Y. Matiks, D. L. Sun, C. T. Lin, A. N. Yaresko, B. Keimer, and A. V. Boris, Nat. Commun. **2**, 219 (2011).
[79] D. J. Scalapino, J. R. Schrieffer, and J. W. Wilkins, Phys. Rev. **148**, 263 (1966).
[80] D. J. Scalapino, in *Superconductivity: In Two Volumes*, Vol. 1, edited by R. D. Parks (Dekker, New York, NY, 1969).
[81] S. V. Borisenko, V. B. Zabolotnyy, D. V. Evtushinsky, T. K. Kim, I. V. Morozov, A. N. Yaresko, A. A. Kordyuk, G. Behr, A. Vasiliev, R. Follath, and B. Büchner, Phys. Rev. Lett. **105**, 067002 (2010).
[82] D. I. Khomskii and F. V. Kusmartsev, Phys. Rev. B **46**, 14245 (1992).